ACS OMEGA

http://pubs.acs.org/journal/acsodf

Article

First-Principles Calculations to Investigate the Stability and Thermodynamic Properties of a Newly Exposed Lithium−Gallium−Iridium-Based Full-Heusler Compound

Md. Arif Ul Islam,* Md. Rasidul Islam, Ovijit das, Shinya Kato, Naoki Kishi, and Tetsuo Soga

Cite This: *ACS Omega* 2023, 8, 21885−21897

Read Online

ACCESS | Metrics & More | Article Recommendations

ABSTRACT: The structural, optical, electrical, thermodynamic, superconducting, and mechanical characteristics of $LiGa_2Ir$ full-Heusler alloys with the $MnCu_2Al$ configuration were comprehensively examined in this work using the first-principles computation approach premised upon density functional analysis. This theoretical approach is the first to investigate the influence of pressure on the mechanical and optical characteristics of $LiGa_2Ir$. The structural and chemical bonding analysis shows that hydrostatic pressure caused a decrease in the lattice constant, volume, and bond length of each cell. According to the mechanical property calculations, the $LiGa_2Ir$ cubic Heusler alloy exhibits mechanical stability. It also has ductility and anisotropic behavior. This metallic substance shows no band gap throughout the applied pressure range. The physical characteristics of the $LiGa_2Ir$ full-Heusler alloy are analyzed in the operating pressure range of 0−10 GPa. The quasi-harmonic Debye model is employed to analyze thermodynamic properties. The Debye temperature (291.31 K at 0 Pa) increases with hydrostatic pressure. A newly invented structure attracted a lot of attention around the globe for its superior superconductivity ($T_c \sim 2.95$ K). Optical functions have also been improved after applying stress to utilize it in optoelectronic/nanoelectric devices. The optical function analysis is supported strongly by the electronic properties. Due to these reasons, $LiGa_2Ir$ imposed an essential guiding principle for relevant future research and could be a credible candidate substance for industrial settings.

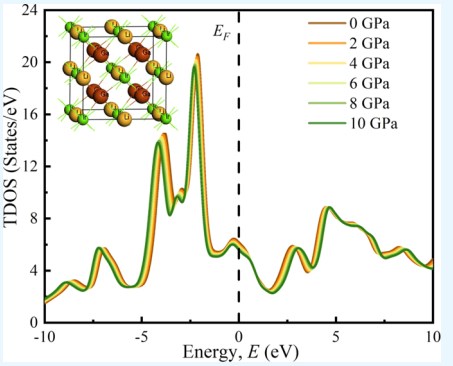

1. INTRODUCTION

Several researchers from all over the world have focused on Heusler metals because of their tunable properties, including their high Curie temp, tunable electronics structure, acceptable semiconducting lattice parameter, and varied magnetic property.[1−9] Heusler alloy intermetallic compounds are attractive options for thermoelectric materials[10−12] and topological insulators.[5,13] They can also be used as shape-memory materials, spin-gapless semiconductors, and other forms of thermoelectric materials.[14−17] Heusler substances can be broadly categorized into half-Heusler, full-Heusler, and last, quaternary-Heusler. These structures' stoichiometric configurations are XYZ, XY_2Z, and XYMZ, in which X, Y, and M are typically transition metals and Z is the leading group component.[18−20] XY_2Z, a full-Heusler configuration, settles in a cubic $L2_1$ arrangement ($MnCu_2Al$-sample) with the spatial group $Fm\bar{3}m$ (# 225).[18,21,22] In this article, we will investigate the physical characteristics of one such type. $LiGa_2Ir$ Heusler is a relatively new intermetallic compound that has attracted attention in the scientific community due to its unique combination of physical and superconducting properties.[21] This material is composed of elements Li (lithium), Ga (gallium), and Ir (iridium) and has a cubic crystal structure. Studying this material under pressure has revealed several interesting properties that have implications for a more comprehensive array of technical purposes.[23−25] Physical properties like crystal structure, thermal conductivity, and electrical conductivity are crucial parameters that determine the material's performance in different applications, which can be predicted computationally.[26,27] The crystal structure of $LiGa_2Ir$ Heusler is found to be sensitive to pressure and undergoes structural transitions at specific pressures.[21] Thermal conductivity is an essential factor that regulates the material's ability to transfer heat and is also found to be pressure-dependent.[28,29] Similarly, the electrical conductivity of $LiGa_2Ir$ Heusler is sensitive to pressure and has been studied under different pressures to determine its behavior. One of the most exciting properties of $LiGa_2Ir$ Heusler is its superconducting behavior, and it is recently studied by Górnicka's team.[21] Superconductivity is a phenomenon where a material demonstrates no electrical resistance and completely expulses magnetic fields underneath a critical temperature (T_c).[30] Bulk superconductiv-

Received: March 14, 2023
Accepted: May 15, 2023
Published: June 5, 2023

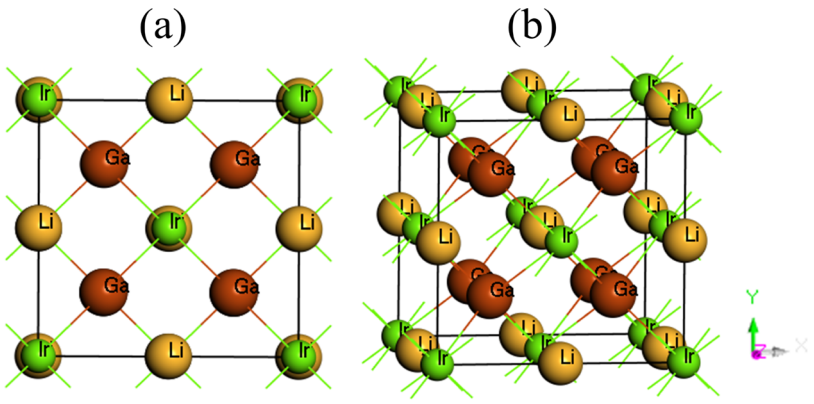

Figure 1. Constructed conventional unit cell of the $LiGa_2Ir$ compound: (a) two-dimensional (2D) and (b) three-dimensional (3D) crystals.

ity is confirmed by the heat capacity, electrical resistivity, and magnetic susceptibility. Theoretical simulations demonstrate that the Fermi surface is influenced by the 5d states of Ir and the 4p states of Ga. The phonon spectrum identified three sets of modes, with the heaviest iridium contributing the most. $LiGa_2Ir$ is an Ir-based superconductor with T_c greater than that of Rh-containing isostructural and isoelectronic compounds. This is due to the stronger electron−phonon coupling constants e−p resulting from the higher Ir versus Rh mass. T_c's reported a modest pressure dependency, which is due to its high bulk modulus, small Grüneisen parameter, and a compensatory increase in electronic contribution. Superconductivity is a phenomenon in which a material demonstrates electrical resistance and complete expulsion of magnetic fields below a critical temperature. This makes $LiGa_2Ir$ Heusler an exciting material for further studies in the field of superconductivity, as the pressure-dependent behavior of its superconducting properties can be used to tune its performance in various applications.[18,21,31] In 2021, Górnicka et al.'s first investigation revealed that the superconducting properties of $LiGa_2Ir$ Heusler, including T_c and critical magnetic field, are found to be pressure-dependent, and the maximum T_c of this material is found to be around 2.95 K. To understand the electronic structure, lattice dynamics, and electron−phonon interaction in $LiGa_2Ir$, the researchers conducted first-principles calculations. The calculated electron−phonon coupling constant (λ_{e-p}) was found to be 0.57, confirming that the superconductivity in $LiGa_2Ir$ is mediated by the electron−phonon mechanism.[21]

In conclusion, $LiGa_2Ir$ Heusler is a promising material for various technological applications due to its combination of physical and superconducting properties sensitive to pressure. Recent studies have revealed several interesting properties of this material, including its crystal structure, thermal conductivity, electrical conductivity, and superconducting properties. These properties make $LiGa_2Ir$ Heusler an exciting subject for further research and its potential applications in various fields such as electronics, energy, and materials science. The pressure-dependent behavior of its properties provides a means to tune its performance for specific applications, making $LiGa_2Ir$ Heusler a material with immense potential. This study is to comprehensively examine the structural, optical, electrical, thermodynamic, superconducting, and mechanical characteristics of $LiGa_2Ir$ full-Heusler alloys with the $MnCu_2Al$ configuration under hydrostatic pressure using the first-principles computation approach. Specifically, this research aims to investigate the influence of hydrostatic pressure on the superconducting, mechanical, and optical properties of $LiGa_2Ir$, analyzes its thermodynamic properties using the quasi-harmonic Debye model, and explores its potential for use in superconducting materials and industrial settings. The pressure effect on this half-Heusler substance can make this one lucrative object in various applicable arenas, utilizing process−property−performance linkages.

2. COMPUTATIONAL METHODS

In this research, the Cambridge Serial Total Energy Package (CASTEP) is employed to predict the physical characteristics of two-dimensional $LiGa_2Ir$ based on the first-principles approaches.[32,33] The orbital geometry conditions are disregarded by the CASTEP algorithm.[33] The correlation and electron interchange energies are calculated using the general gradient approximations (GGAs) by Perdew−Burke−Ernzerhof (PBE) and PBEsol.[34] Consideration is given to the ultrasoft-pseudopotential that resembles Vanderbilt's and facilitates electron−ion interaction.[35] To enhance LDA, Hohenberg and Kohn argued that the gradients of local density should be included in the formula for exchange with correlation. The latter serves as the basis for GGA, whereby the exchange−correlation density is influenced by both the electronic density gradient $\nabla n(r)$ and the electronic density $n(r)$ alone.[36,37] The LDA density of energy is primarily changed to produce the exchange−correlation energy in GGA, which may be shown as

$$E_{xc}^{GGA} = \int n(\mathbf{r})\varepsilon_{xc}^{GGA}[n(\mathbf{r}), \nabla n(\mathbf{r})]d\mathbf{r} = \int \varepsilon_x^{hom} n(\mathbf{r})F_{xc}[n(\mathbf{r}), \nabla n(\mathbf{r})]n(\mathbf{r})d\mathbf{r} \quad (1)$$

The exchangeable energy density of an evenly distributed electron gas with a density of $n(r)$ is denoted by the symbol. The one-dimensional parameter F_{xc} is gradient and density-dependent. The two subcategories of F_{xc} are exchange and correlation. The structural relaxation was attained using the LBFGS minimization procedure. The test used $LiGa_2Ir$ primitive units with a 600 eV plane-wave cutoff energy. A Monkhorst−Pack framework with 364 intricate K-points (24 × 24 × 24) was employed to sample the Brillouin zone.[21] The elastic constants are computed using finite strain theory, implemented in the CASTEP segment.[32,33] The highest strain amplitude stayed set at 0.003. Maximum displacements of 0.001 Å, the extreme stress of 0.05 GPa, the highest forces of 0.03 eV/Å, and the total energy of 1×10^{-5} eV/atom are the considerations for geometry optimization convergence thresholds.[32,33] With a maximum of 100 repetitions, the electronic self-consistent field tolerance was adjusted to 5×10^{-7} eV/atom. The charge is set to 0.5, and the

https://doi.org/10.1021/acsomega.3c01534
ACS Omega 2023, 8, 21885−21897

spin is set to 2.0 in the Pulay charge density mixing method. The CASTEP tool subtracts the optical attributes established on the standard DFT Kohn–Sham orbitals.[38,39]

3. RESULTS AND DISCUSSION

3.1. Structural Properties. The $LiGa_2Ir$ superconductor, a member of the complete Heusler phase, has a cubic crystal structure with the $Fm\bar{3}m$ spacing group (No. 225).[21] A three-dimensional representation of the $LiGa_2Ir$ crystal lattice is shown in Figure 1, employing the Visualization for Electronic Structural Analysis (VESTA) software.[40] Cubic $LiGa_2Ir$ superconductor is present in 16 and 4 atoms in the ordinary conventional cells and primitive cells of Figure 1, respectively. The Ga atoms are situated at 8c Wyckoff positions (0.25, 0.25, 0.25), whereas Li and Ir are in 4a Wyckoff locations (0, 0, 0) and 4b Wyckoff positions (0, 0, 0.5), respectively.[21] The Heusler $LiGa_2Ir$ superconductor's assessed values for the lattice constant (a) and unit cell volumes (V) at an applied pressure range from 0 to 10 GPa, as well as any known experimental and other theoretical data, are shown in Table 1.

Table 1. Theoretical and Experimental Values of the Lattice Constant *a* and the Measured Volume of a Unit Cell *V* of $LiGa_2Ir$ at Various Pressures

	a (Å)				
pressure (GPa)	this work (PBE)	this work (PBEsol)	other works (PBEsol)	experimental (pXRD)	*V* (Å^3) (PBE)
0	6.068	6.011	6.016[21]	6.032[21]	223.43
2	6.039	5.985			220.24
4	6.011	5.960			217.19
6	5.985	5.936			214.38
8	5.961	5.914			211.82
10	5.938	5.893			209.37

The processed lattice parameters are in excellent understanding with the outcomes of experiments.[21] The lattice parameter was determined via PBE and PBEsol. With PBEsol interchange–correlation functional, the calculated value at 0 GPa is clearly closer to the data collected from experiments (0.3% error) compared to the PBE interchange–correlation functional (0.6% deviation). So, the crystal parameters are analyzed from 0 to 10 GPa with the PBEsol exchange–correlation function. This demonstrates the correctness and dependability of the present first-principles calculations that are DFT-based.[39] With the applied pressure, lattice volume (V), and lattice parameter (a) decrease, this also fits well with the experimentation.[21] As pressure increases, we see a reduction in lattice parameters and volume. This means that the space between atoms is decreasing. This causes the repulsive effects between atoms, increasing the crystal compression under high pressure. This is the first study to evaluate the impact of pressure on $LiGa_2Ir$, and it has not been possible to perform a comparison with other studies.

3.2. Electronic Properties. Electronic band spectrum, total and partial densities of states (TDOS and PDOS), bond length, and charge density are valuable tools for discussing and interpreting a material's electronic structure and properties.[41,42] The valence and conduction band electrons within the materials determine all of the important properties of solids. The type of energy dispersion in the Brillouin zone area affects these electrons' behavior. Figure 2 depicts the $LiGa_2Ir$ band topologies at 0 and 10 GPa, respectively. The valence band (VB) and the conduction band (CB) are represented, while horizontally dotted lines at 0 eV show the Fermi level. At zero pressure, the high symmetrical point of the initial Brillouin zone of $LiGa_2Ir$ is metallic (Figure 2). $LiGa_2Ir$ has a coincident valence band maxima (VBM) and conduction band minima (CBM). It stays metallic when pressures between 0 and 10 GPa are applied. The primary need for a superconductor is making the structure of the metal. It is shown that $LiGa_2Ir$ has this property using the GGA-PBE approximation.[34] To determine the $LiGa_2Ir$ structure's bonding characteristics, which are shown in Figure 3, the TDOS and PDOS have been determined.[43,44]

Figure 3 shows two VBs intersecting the E_F, located on a TDOS curve with a falling slope. In Figure 4, the contribution of every element's orbital in the density of states and hybridization is discussed. The Ga-4p and Ir-5d states make up the majority of the contribution at E_F. At E_F, Li contributes very little. This study shows that these electrons are primarily responsible for superconductivity in $LiGa_2Ir$, as seen in earlier studies.[21] At E_F DOS levels, $LiGa_2Ir$ has 1.56 states/eV/fu, which is in good pact with previous hypothetical studies.[21] This value does not change in any significant way with the applied hydrostatic pressures.

A possible technique to examine a material's chemical bonding structure is the Mulliken atomic population.[45,46]

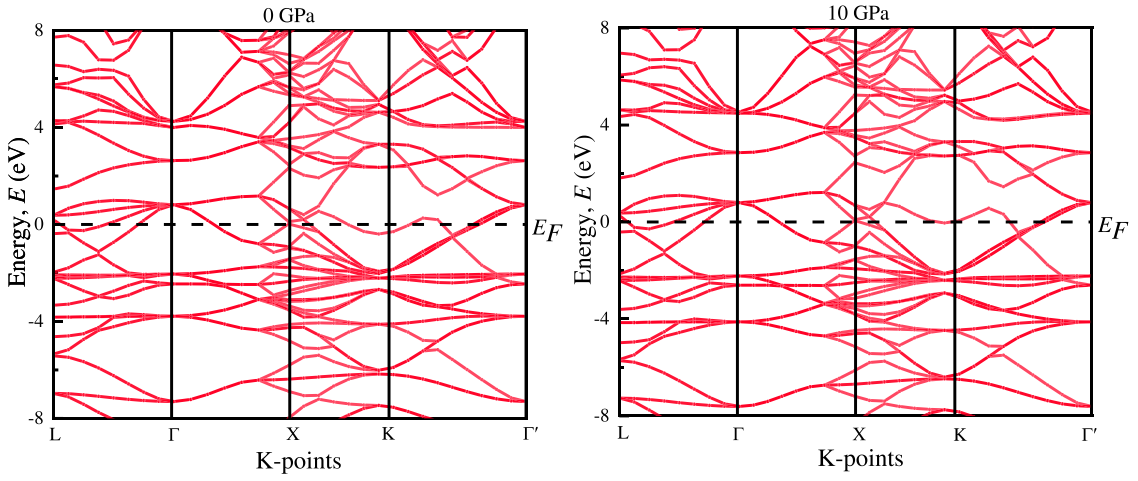

Figure 2. Electronic band structure computed of $LiGa_2Ir$ at 0 and 10 GPa pressures.

https://doi.org/10.1021/acsomega.3c01534
ACS Omega 2023, 8, 21885−21897

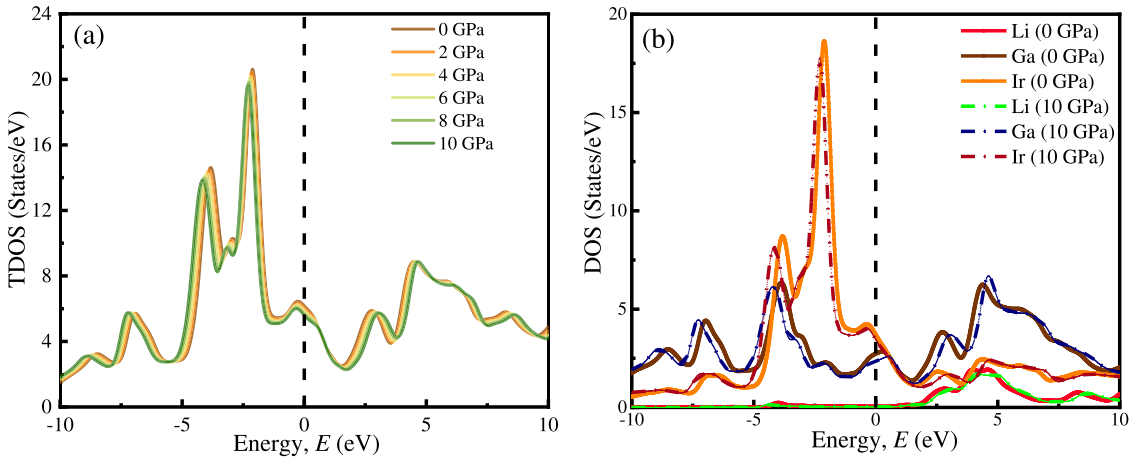

Figure 3. Calculated (a) TDOS of the $LiGa_2Ir$ compound at 0, 2, 4, 6, 8, and 10 GPa and (b) DOS of Li, Ga, and Ir atoms in the $LiGa_2Ir$ compound at 0 and 10 GPa pressures.

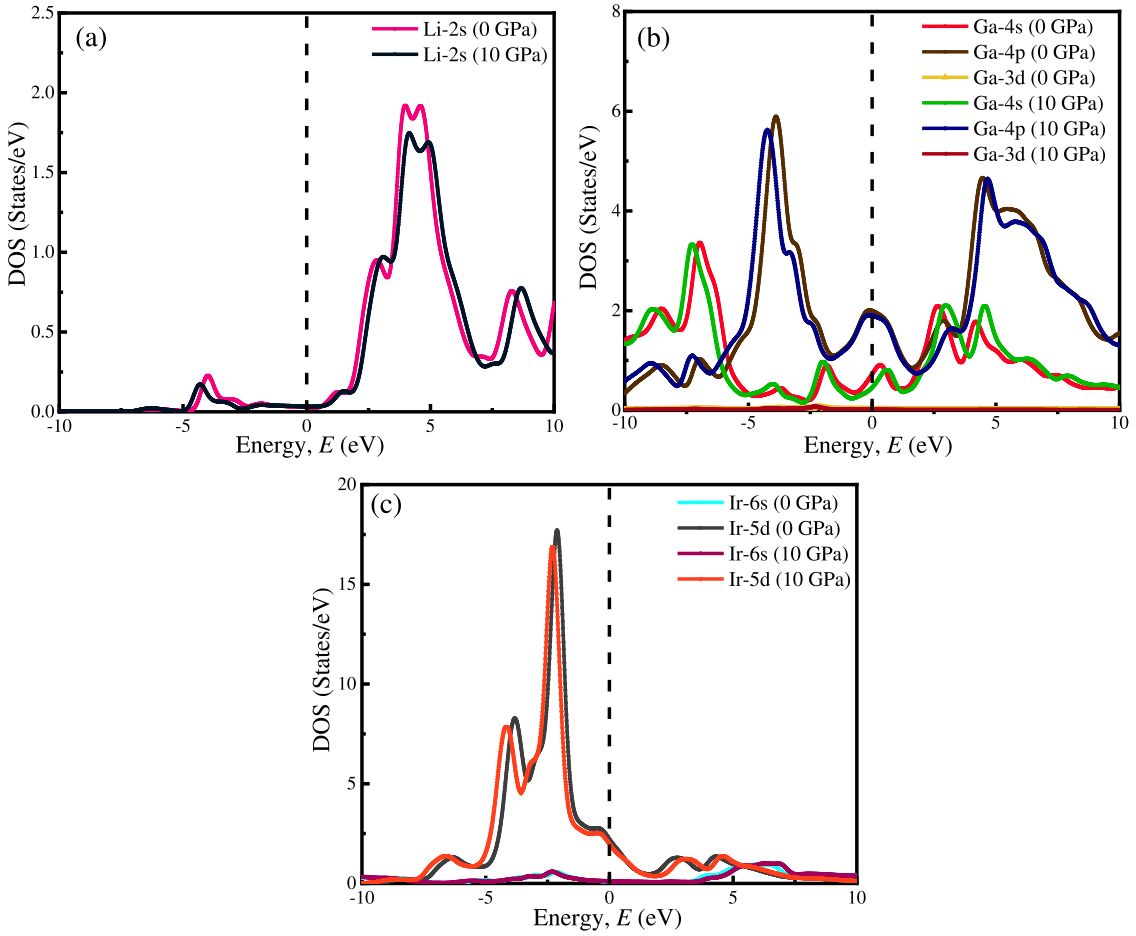

Figure 4. Calculated PDOS: (a) Li, (b) Ga, and (c) Ir of $LiGa_2Ir$ at 0 and 10 GPa pressures.

Table 2. Mulliken Atomic Populations of the $LiGa_2Ir$ Superconductor

compound	P (GPa)	species	s	p	d	total	charge	bond	population	length (Å)
$LiGa_2Ir$	0	Li	1.54	0.00	0.00	1.54	1.46	Li−Ga	−0.79	2.628
		Ga	1.24	2.14	9.99	13.38	−0.38			
		Ir	0.58	1.01	8.11	9.71	−0.71	Ga−Ir	0.13	2.628
	10	Li	1.47	0.00	0.00	1.47	1.53	Li−Ga	−0.77	2.572
		Ga	1.17	2.20	9.99	13.36	−0.36			
		Ir	0.57	1.11	8.12	9.81	−0.81	Ga−Ir	0.13	2.572

https://doi.org/10.1021/acsomega.3c01534
ACS Omega 2023, 8, 21885−21897

When a material exhibits electrostatic attraction, which means ionic bonding, the bond population is low, but when a material shows covalent bonding, the bond population is large.[47] Table 2 displays the $LiGa_2Ir$ superconductor's computed bond populations. Table 2 indicates that Ga and Ir have negative charges for the $LiGa_2Ir$ superconductor. This means that the positive charges of Li atoms are now transferred to Ga or Ir. Because the Ga−Ir link has a positive bond population of 0.13 at both maximum and minimum stresses 0 and 10 GPa, a strong covalent contact is exhibited between the Ga and Ir atoms (Table 2). In contrast, the Li−Ga (Li−Ga) bond's bond population is negative (0.79 (0.77) at 0 (10) GPa), indicating ionic bonding properties. The Li−Ga (Ga−Ir) bond length is 2.628 (2.572) Å. Last but not least, it has been shown that these substances include ionic and covalent bonds by careful investigation and computation of the cumulative/total DOS, PDOS, Mulliken atomic populations, and total charge distribution of the $LiGa_2Ir$ superconductor. This is a shared trait of structural materials of the $MnCu_2Al$ class.

3.3. Mechanical Properties. The elastic factor is a crucial measurement system for understanding the mechanical attributes, stability, internal forces in solids, and stiffness of materials.[48,49] Elastic and mechanical attributes are critical considerations in materials engineering concerning the improvement and use of appliances.[18] Consequently, finite strain theory is used to survey the mechanical attributes.[23] Understanding how hydrostatic pressure influences the elastic constants is vital since the lattice parameter of $LiGa_2Ir$ decreases with imposed hydrostatic pressure. Three distinct elastic variables within crystals are C_{11}, C_{12}, and C_{44}. Table 3 displays the $LiGa_2Ir$ superconductor-calculated elastic constants for different pressures. The Born stability criteria mentioned below[50] determine the mechanical stability of the phase

$$C_{11} > 0,\ C_{44} > 0,\ C_{11} + 2C_{12} > 0 \text{ and } C_{11} - C_{12} > 0 \tag{2}$$

It is clear from Table 3 that these projected elastic constants fulfill every one of the Born stability constraints, which confirms the mechanical stability of the investigated material. It is feasible to ascertain if a material is ductile (+ve/positive value) or brittle (−ve/negative value), employing the Cauchy pressure ($C_{11}-C_{44}$).[23,26] In Table 3, the estimated Cauchy pressure is tabulated, and it can be observed that both compounds' computed values are positive under all applied stresses, revealing that they are ductile. With heightened pressure, materials become more ductile (see Table 3). Fundamental mechanical parameters of $LiGa_2Ir$, like the bulk modulus (B) as well as shear modulus (G), are calculated from the likely elastic constants C_{ij} using the Voigt−Reuss method. This method is described in the article published by the journal.[51]

As well, the following formulations[51] are managed to determine Young's modulus (E) and Poisson's ratio (υ)

$$E = \frac{9GB}{3B + G} \tag{3}$$

$$\nu = \frac{3B - 2G}{2(3B + G)} \tag{4}$$

Corresponding to Table 4, the increasing pressure intensifies the quantities of B, G, and E, proving that doing so increases the hardness of $LiGa_2Ir$ material. As the hydrostatic pressure increases, the lattice parameter declines, expanding the substance's stiffness by diminishing the interatomic space. This is significant to the increase in B, G, and E, which increases hardness. The $LiGa_2Ir$ substance is a particularly hard material since its predicted bulk modulus is comparably large (>100 GPa). Due to the larger value of B, the $LiGa_2Ir$ compound exhibits a significant impedance to volume shift at a given stress. The system used to represent the Voigt−Reuss constraints for the bulk modulus, as well as the shear modulus, continues to follow

$$B_V = B_R = \frac{C_{11} + 2C_{12}}{3} \tag{5}$$

$$G_V = \frac{C_{11} - C_{12} + 3C_{44}}{5} \tag{6}$$

$$G_R = \frac{5C_{44}(C_{11} - C_{12})}{[4C_{44} + 3(C_{11} - C_{12})]} \tag{7}$$

The stages Hill got to regulate B and G are shown hereafter

$$B_H = B = \frac{1}{2}(B_R + B_\nu) \tag{8}$$

$$G_H = G = \frac{1}{2}(G_\nu + G_R) \tag{9}$$

Statistics of a substance's ductile/brittle role include Pugh's ratio (B/G) and Poisson's ratio (υ).[52] The boundary values of B/G and υ, which are 1.75 and 0.25, respectively, in that order, signify

Table 3. Estimated Quantities of C_{ij} (GPa) and Cauchy Pressure $C_{12}-C_{44}$ (GPa) of the $LiGa_2Ir$ Superconductor at Various Pressures

pressure (GPa)	C_{11}	C_{12}	C_{44}	C_{12}-C_{44}	remarks
0	166.6	138.8	82.7	56.1	31
0	145.67	118.22	91.31	26.91	this work
2	158.65	130.96	95.56	35.40	this work
4	166.95	139.19	99.59	39.60	this work
6	181.64	153.64	104.14	49.50	this work
8	190.99	162.82	107.64	55.18	this work
10	200.95	172.63	111.20	61.43	this work

Table 4. Mechanical Properties Calculated of $LiGa_2Ir$ at Various Pressures

pressure (GPa)	B (GPa)	G (GPa)	E (GPa)	(B/G)	ν	A^U	remarks
0	148.07	41.47	113.79	3.57	0.372	5.95	31
0	127.37	44.14	118.70	2.89	0.345	6.65	this work
2	140.19	45.65	123.55	3.07	0.353	6.90	this work
4	148.44	47.00	127.55	3.16	0.357	7.18	this work
6	162.97	48.61	132.63	3.35	0.364	7.44	this work
8	172.21	49.83	136.33	3.46	0.368	7.64	this work
10	182.07	51.05	140.07	3.57	0.372	7.85	this work

https://doi.org/10.1021/acsomega.3c01534
ACS Omega 2023, 8, 21885−21897

Table 5. Minimum and Maximum Values of Young's Modulus, Compressibility, and Shear Modulus, as well as Poisson's Ratio and the Ratio A of $LiGa_2Ir$

P (GPa)	Y_{min} (GPa)	Y_{max} (GPa)	A_Y	K_{min} (TPa^{-1})	K_{max} (TPa^{-1})	A_K	G_{min} (GPa)	G_{max} (GPa)	A_G	ν_{min}	ν_{max}	A_ν	remarks
0	36.44	136.91	3.76	3.08	3.08	1.00	12.62	53.11	4.21	−0.237	0.987	∞	18
0	39.73	221.09	5.56	2.62	2.62	1.00	13.72	91.31	6.66	−0.435	1.164	∞	this work
10	41.39	277.15	6.70	1.83	1.83	1.00	14.16	111.19	7.86	−0.486	1.277	∞	this work

the ductile/brittle nature.[53] A material is considered to be ductile when the B/G ratio of its material is higher than its marginal value. If it is not, it is considered to be brittle.[53] The structure is ductile at all pressures ranging from 0 to 10 GPa based on the calculated value of B/G (see Table 4), and they develop more ductile with boosting pressure. The value of Poisson's ratio (υ) must be in the range of 0.25 and 0.5.[53] Table 4 demonstrates that the magnitude exists around 0.25 and 0.5 throughout the entire operating pressure, representing the presence of a central force within the $LiGa_2Ir$ substance. We also calculated the substances' elastic anisotropic (A) factor, which offers crucial details about how the medium performs in real-world situations.[54,55] It is calculated using the Zener equation,[56] which is provided below and shown in Table 5

$$A^U = \frac{2C_{44}}{C_{11} - C_{12}} \tag{10}$$

The $LiGa_2Ir$ superconductor demonstrates anisotropic performance due to $A^U > 1$ (Table 5). The following equation is essential for resolving the anisotropic behavior of a substance. In the presence of pressure, $LiGa_2Ir$ shows significant anisotropy. This indicates that mechanical characteristics are dependent upon the direction.

The ELATE tool[57] was used to highlight the dependence of Young's modulus (E), Poisson's ratio (υ), and shear modulus (G) at 0 and 10 GPa stresses for further clarification of the anisotropic nature (shown in Figures 5 and 6). The cyclic 2D and 3D charts show comprehensive isotropy, and their aberrations represent a matter's anisotropic nature. The assessed compound exhibits anisotropic characteristics in every course, as is found in the 3D diagrams. Additionally, the deviation in 3D spherical for a 10 GPa pressure is less intense than for 0 GPa. This means that the inducing pressure cannot significantly increase the anisotropic quality.

3.4. Thermodynamic Properties. Functional materials can be utilized at various temperatures and pressures. Therefore, it is essential to understand how thermodynamic parameters such as temperature and pressure affect the ability to use these materials in engineering applications. The temperature when a crystal shows its most excellent regular mode of vibrations is called the Debye temperature.[58,59] Melting points, heat capacity, thermal conductivity, and Dulong−Petit limits are only a few of the essential qualities significantly influenced by the investigation of such a Debye temperature, a somewhat thermodynamic property.[60,61] The creation of linked materials depends on this assessment. Accurate determination of the Debye temperature seems difficult. The mathematically measured value may differ from the actual finding in several situations.[62] We utilized data on the expected elastic moduli to get the Debye temperature for $LiGa_2Ir$. The averaged sound velocity (V_m), longitudinal sound velocity (V_l), and transversal sound velocity (V_t) are used to compute the Debye temperature, as stated in the following formula[63]

$$\Theta_D = \frac{h}{k_B}\left(\frac{3N}{4\pi V}\right)^{1/3} \times \nu_m \tag{11}$$

$$\nu_m = \left[\frac{1}{3}\left(\frac{2}{\nu_t^3} + \frac{1}{\nu_l^3}\right)\right]^{-1/3} \tag{12}$$

$$\nu_l = \left(\frac{3B + 4G}{3\rho}\right)^{1/2} \tag{13}$$

And

$$\nu_t = \left(\frac{G}{\rho}\right)^{1/2} \tag{14}$$

The computed V_m, V_υ, V_l, ρ, and Θ_D for $LiGa_2Ir$ superconductors are shown in Table 6 from 0 to 10 GPa. With increasing pressure, the values of density, V_m, V_υ, V_l, and Θ_D increase. From the work of Górnicka et al.,[21] Θ_D was found to be 277 K and the experimental results are higher than the theoretically calculated Debye temperature value at 0 GPa. It is hard to accurately measure Debye temperatures. Many cases show greater variation between experimental and theoretical Debye temperatures.[62,64] Table 6 indicates that Debye's temperature increases with increasing pressure. This is due to the stronger interatomic bonding. This is confirmed by the decreased bond length and lattice constant with pressure.

The capacity of materials to transfer thermal energy from one area to the next is known as thermal conductivity. The lowest thermal conductance is a significant thermodynamic characteristic (K_{min}). As temperatures increase, the materials' thermal conductivity diminishes until it ultimately falls to what is referred to as the lowest thermal conductivity. The minimal conductivity of the superconductive material is calculated by utilizing the following formula[18]

$$K_{min} = k_B \nu_m \left(\frac{M}{n\rho N_A}\right)^{-2/3} \tag{15}$$

where k_B is stated as the Boltzmann constant, M denotes molecular mass, n is the magnitude of atoms per molecule, N_A is demarcated as Avogadro's number, and ρ is the density.

By using the Clarke formula, Table 7 displays the $LiGa_2Ir$ superconductor's computed K_{min}. The K_{min} is determined by the interactions between molecules and atoms in the materials. These samples are more densely packed at higher pressures, which can lead to stronger interatomic bonding. These bonds create barrier phonons from moving. This causes the material's thermal conductivity to increase with increasing pressure. Its melting point is another crucial thermodynamic variable that is crucial to thermodynamics. The melting temperature, T_m, of the cubic-type crystal may be determined using the following equation[18]

$$T_m = 553 + 5.91C_{11} \pm 300\ \text{K} \tag{16}$$

https://doi.org/10.1021/acsomega.3c01534
ACS Omega 2023, 8, 21885−21897

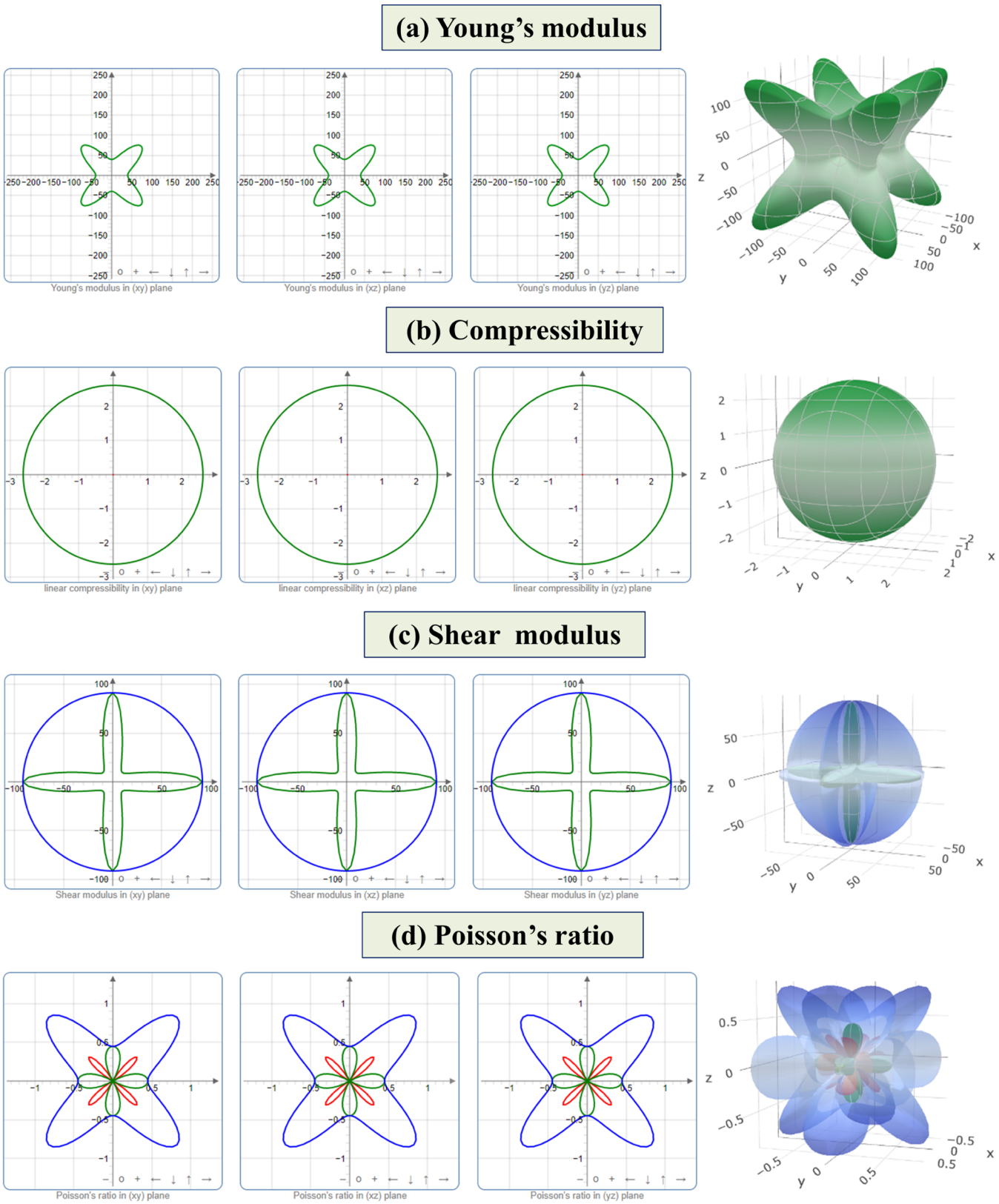

Figure 5. 3D and 2D diagrams of (a) Y, (b) K, (c) G, and (d) ν of $LiGa_2Ir$ at 0 GPa.

The predicted melting point for $LiGa_2Ir$ is shown in Table 7 from 0 to 10 GPa. Because of stronger interatomic bonding, melting temperatures increase with pressure. At extreme temperature, the anharmonic effect of specific heat at a constant volume is reduced. The Dulong–Petit limit is a value that is near the cutoff. The Dulong–Petit limit may be assessed as follows[65]

$$\text{Dulong–Petitlimit} = 3nN_Ak_B \quad (17)$$

https://doi.org/10.1021/acsomega.3c01534
ACS Omega 2023, 8, 21885−21897

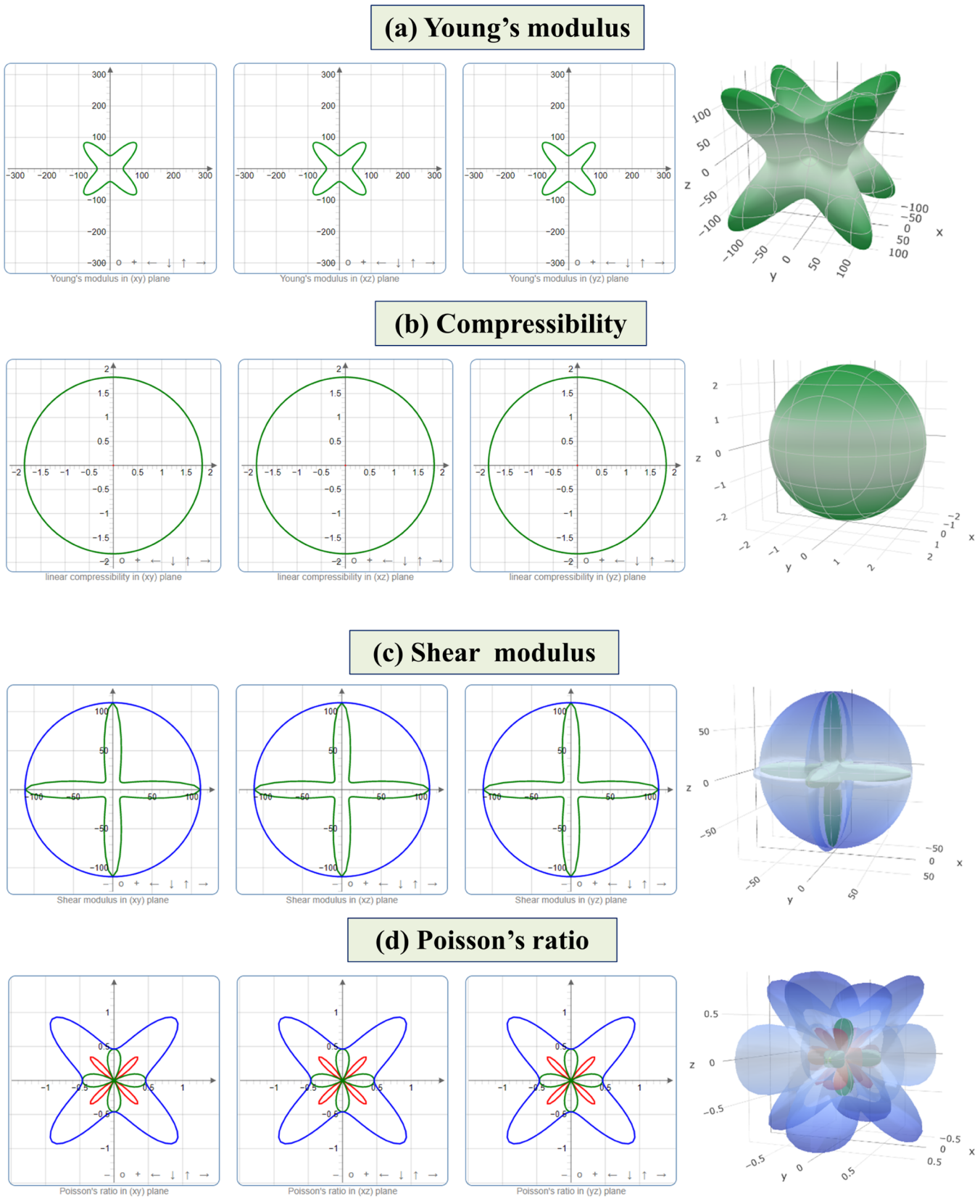

Figure 6. 3D and 2D diagrams of (a) Y, (b) K, (c) G, and (d) ν of $LiGa_2Ir$ at 10 GPa.

where k_B stands for the Boltzmann constant and N_A stands for Avogadro's constant. The Dulong–Petit limit for the cubic $LiGa_2Ir$ superconductor is determined using eq 17.

3.5. Superconducting Properties. The term "superconductors" refers to substances that carry electricity without encountering any resistance.[66−68] The quantum confinement of superconductors is still a mystery even after a century after its

https://doi.org/10.1021/acsomega.3c01534
ACS Omega 2023, 8, 21885−21897

Table 6. Calculated Density (ρ) as well as Transverse (V_t) Velocity, Longitudinal (V_l) Velocity, and Average Sound Velocity (V_m) and Debye Temperature (Θ_D) of the $LiGa_2Ir$ Superconductor

pressure (GPa)	ρ (gm/cm^3)	V_t (m/s)	V_l (m/s)	V_m (m/s)	Θ_D (K)	remarks
0					277	21
0	10.07	2093.64	4300.34	2352.22	291.31	this study
2	10.22	2113.46	4435.41	2377.20	295.73	this study
4	10.36	2129.95	4514.10	2396.93	299.56	this study
6	10.50	2151.63	4657.64	2423.82	304.33	this study
8	10.62	2166.12	4740.44	2441.37	307.49	this study
10	10.75	2179.18	4823.75	2457.35	310.98	this study

Table 7. Computed Minimum Thermal Conductivity (K_{min}) as well as Melting Temperature (T_m) and the Dulong–Petit Limit of the $LiGa_2Ir$ Superconductor

pressure (GPa)	K_{min} (W/(m K))	T_m (K)	Dulong–Petit limit (J/mol·K)	remarks
0	0.44	1291.75	99.74	18
0	0.56	1413.91	99.69	this study
2	0.57	1490.62		
4	0.58	1539.67		
6	0.59	1626.49		
8	0.60	1681.75		
10	0.61	1740.61		

discovery; therefore, the quest for novel superconducting materials is quite intriguing. The superconducting critical temperature (T_c), the electron–phonon coupling constant (λ), and the Coulomb coupled constant are all related according to McMillan's famous strong-coupled model of superconducting materials.[69] A theoretical connection for determining T_c directly is as follows[70]

$$T_c = \frac{\theta_D}{1.45} e^{-1.04(1+\lambda)/\lambda - \mu^*(1+0.62\lambda)} \quad (18)$$

where the electron–phonon coupling constant, the Debye temperatures, and Coulomb pseudopotential, respectively, are λ, θ_D, and μ^*.

The μ^*, a constraint range that can be modified from 0.1 to 0.15, is judged as physically satisfactory.[70,71] The Coulomb pseudopotential μ^* is established in eq 19 as follows

$$\mu^* = 0.26\frac{N(E_F)}{1 + N(E_F)} \quad (19)$$

It can be seen that the value μ^* does not have an impact with pressure. However, the value of DOS at the Fermi level $N(E_F)$ of $LiGa_2Ir$ stays nearly constant as pressure increases. The definition of λ is $N(E_F) \times V_{e-ph}$, where V_{e-ph} represents the electron–phonon interaction energies. Figure 3 shows that the $N(E_F)$ exhibits a slight variation as a function of increasing applied pressure. In the current study, the variation of λ is affected by the effect of V_{e-ph} on the applied pressure. According to McMillan's equation, for a fixed λ value of this compound, T_c could increase with pressure because of an increasing trend of the Debye temperature. The variance is influenced by the pressure's potential impact on V_{e-ph}. Because of the increasing tendency of θ_D, with pressure, it is predicted from the McMillan formula that for a constant value of the $LiGa_2Ir$ substance, T_c may increase with the imposed pressure. This is possible because the Debye temperature is linearly related to T_c. This suggests that the value for low T_c (T_c > 2.95 K) in the $LiGa_2Ir$ superconductor compounds will increase with the pressure applied to maintain a constant electron–phonon coupling coefficient. Researchers will be fascinated by the exciting properties of $LiGa_2Ir$ when pressure is applied to superconducting materials, both experimentally and theoretically.

3.6. Optical Properties. The optical properties of a superconducting substance are attractive due to its remarkable nature. They show promising results in photovoltaics and optoelectronics.[27,58] This section investigates and provides a detailed analysis of a few optical characteristics. The results are shown at pressures of 0–10 GPa for $LiGa_2Ir$. To calculate additional optical parameters, the dielectric function must first

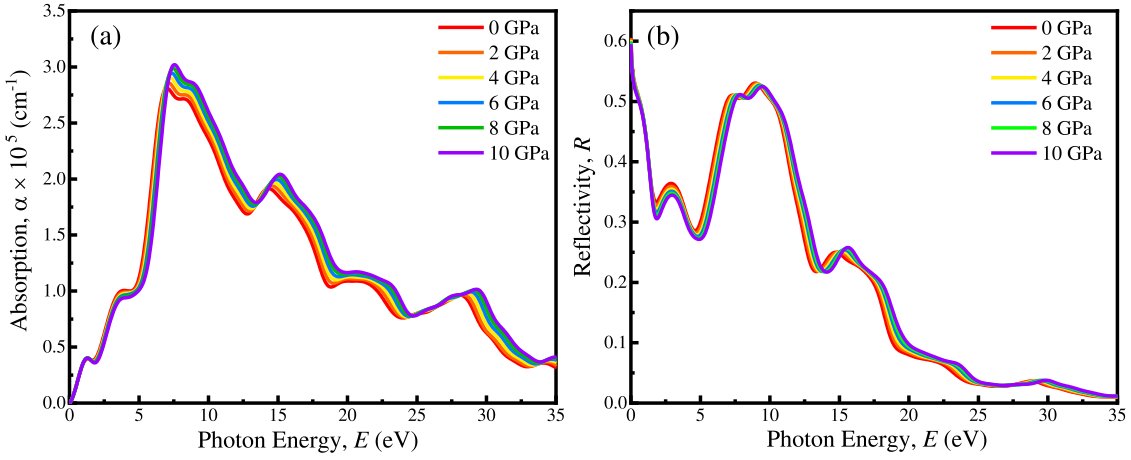

Figure 7. Optical functions of (a) absorption and (b) reflectivity of $LiGa_2Ir$ under different pressures.

https://doi.org/10.1021/acsomega.3c01534
ACS Omega 2023, 8, 21885–21897

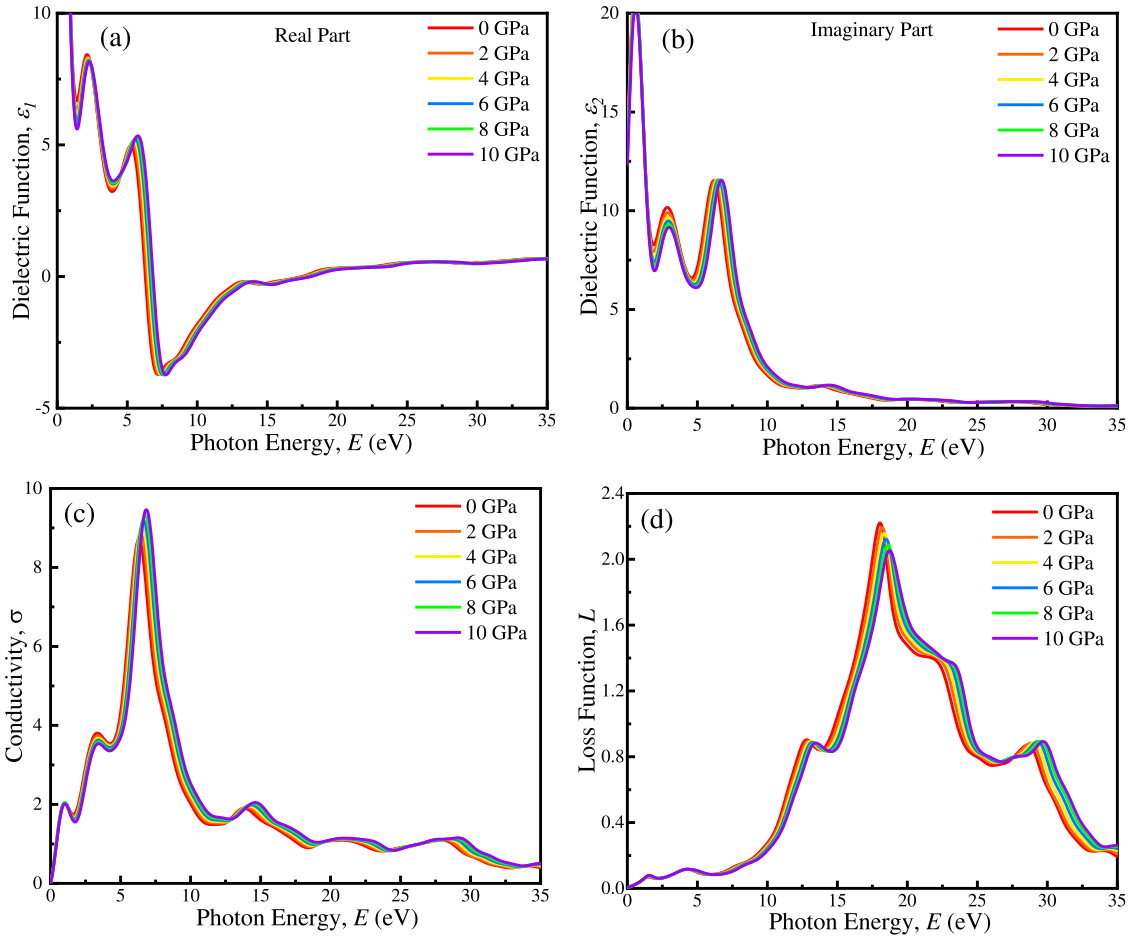

Figure 8. Optical functions of (a) the real part of the dielectric function and (b) the imaginary part of the dielectric function, (c) conductivity, and (d) loss function of $LiGa_2Ir$ under different pressures.

be established.[72] The formula is $\varepsilon(\omega) = \varepsilon_1(\omega) + i\varepsilon_2(\omega)$, where $\varepsilon_1(\omega)$ and $\varepsilon_2(\omega)$ stand for the real and imaginary parts of the dielectric function, correspondingly.[73] Utilizing the Kramers–Kronig relation, it may be determined.[74] The following is a derivation of $\varepsilon_1(\omega)$

$$\varepsilon_1(\omega) = 1 + \frac{2}{\pi} P \int_0^\infty \frac{\omega'^{\varepsilon_2}(\omega')}{\omega'^2 - \omega^2} d\omega' \tag{20}$$

Additionally, $\varepsilon_2(\omega)$ may be developed using the momentum tensors between occupied and unoccupied wave functions[23,26]

$$\varepsilon_2(\omega) = \frac{2e^2\pi}{\Omega\varepsilon_0} \sum_{K,V,C} |\langle \psi_k^c | \hat{U}\cdot\vec{r} | \psi_k^V \rangle|^2 \delta(E_K^C - E_K^V - E) \tag{21}$$

The symbol for the beam's frequency is ω. The wave functions at k for the conduction and valence bands are denoted by ψ_k^c and ψ_k^V, respectively, in that order. Here, e stands for the electronic charge, for the molar volume Ω, and U for the unit vector along the orientation of the input electric field. The delta system preserved the momentum and energy during a transition between occupied and unoccupied electronic states by emitting or absorbing photon energy (E). In addition, at a specific k-vector, E_K^C and E_K^V stand for the electron's energy in the valence and conduction bands, respectively. The formulas used to determine the additional optical properties are covered elsewhere.[75] In this article, we examined the most common optical functions like optical absorption (α), reflectivity (R), loss function, real and imaginary elements of refractive index, optical conductivity (σ), and real (ε_1) and imaginary (ε_2) components of dielectric functions.

The quantity of light energy absorbed into a particular substance is measured by the absorption coefficient.[75] The analyzed absorption spectra for the cubic-structured $LiGa_2Ir$ superconductor are shown in Figure 7a. As the photon energy increases, optical absorption begins to increase. It reaches a peak at 6–8 eV. Then, it starts to fall slowly. It is interesting to observe that external pressure does not significantly impact absorption. The absorption spectrum peak shifts to higher energy as external pressure increases. This illustrates how the $LiGa_2Ir$ combination has a metallic quality. Also, we can get the idea of absorption and from the absolute value of the absorption of the Beer–Lambert law ($A = \alpha cl = -\log(T)$), where A is absorbance, α is the absorption coefficient, c is the concentration of the absorbing portions in the experimenting sample, l is the length, and T is the transmittance. The material's reflectance, a gauge of its suitability for usage as reflectors in real-world gadgets, demonstrates how beneficial it is.[75] The reflectivity spectra of the investigated chemicals are shown in Figure 7b. The reflectance of this compound reduces as photon energy increases. There has been a nonlinear reduction. The reflectivity spectrum has a few peak regions. Both the visible and infrared areas of the electromagnetic continuum have high reflectivity. It progressively drops in the UV area, reaching virtually nothing at 25 eV. Other superconducting compounds in the same family

https://doi.org/10.1021/acsomega.3c01534
ACS Omega 2023, 8, 21885–21897

exhibit behavior reasonably similar to the observed behavior.[25] The responsiveness of a substance to an electromagnetic wave is described by its dielectric property. The real and imaginary components of the $LiGa_2Ir$ superconductor's dielectric properties are shown in Figure 8a,b. The ability of a material to store electrical energy in an electric field is determined by its dielectric constant. In comparison to the nonpressurized configuration, as shown in Figure 8a,b, pressure results in only slightly enhanced real and imaginary parts of the dielectric constant for this material. Normally, the metallic sample under pressure can experience a decrease in the distance between atoms, which can result in a slight increase in the frequency of oscillation of the free electrons. However, the dielectric constant of the metal was not considerably affected by this increase in frequency. As a result, the dielectric constant of this sample remained nearly the same as the pressure increased. There are a few modest spikes in the imagined portion of the dielectric function, yet there is no substantial peak in the actual part of the dielectric feature for this compound. The imaginary portion of the dielectric constant for the $LiGa_2Ir$ combination zeros out at around 20 eV. These statistics imply that the chemical will appear above the corresponding energy levels. For the $LiGa_2Ir$ superconductor, the imaginary portions of the dielectric values from 0 to 20 eV are nonzero, suggesting that absorption occurs throughout this energy range. $LiGa_2Ir$ has a high static dielectric property, which suggests that it may be employed as a dielectric layer.[73] Figure 8c shows the optical conductance of the $LiGa_2Ir$ crystal as a function of the photon energy. Optical conductivity is another name for photoconductivity. In the visible spectrum, the optical conductivity increases quickly, peaking at 1 and 3.2 eV photon energies. In the UV region, conductance reaches its maximum peak at around 6 eV. The conductivity after that started to decline. The majority of metallic compounds have this quality. The loss function is an optical measurement that defines the amount of energy that is lost by a speedy electron when it travels through a substance. Plasma energy refers to the amount at which the loss function is at its highest. At this point, the plasma energy is when the plasmons are excitation and the absorption and reflectivity as well as photoconductivity are reduced dramatically.[76] The plasma frequencies of the $LiGa_2Ir$ superconductor are shown in Figure 8d, which are around 18 eV. As pressure increases, the peak of the loss function shifts toward the higher energy.

4. CONCLUSIONS

In a nutshell, $LiGa_2Ir$ Heusler is a novel intermetallic compound that exhibits a combination of structural, electronic, mechanical, superconducting, and optical properties that make it a promising material for various technological applications such as micro- and nanoelectronics. Its crystal structure properties, such as the lattice volume, lattice parameter, and bond lengths, are found to be sensitive to pressure and undergo structural transitions at specific pressures. The material also has pressure-dependent electrical conductivity, thermal conductivity, and superconducting properties, including a critical temperature. Furthermore, $LiGa_2Ir$ Heusler is found to exhibit interesting optical properties, such as a strong absorption in the infrared region, which makes it a potential candidate for optoelectronic devices. The pressure-dependent behavior of the properties of $LiGa_2Ir$ Heusler provides a means to tune its performance for specific applications, making it a highly versatile material. The combination of its structural, electronic, mechanical, superconducting, and optical properties makes $LiGa_2Ir$ Heusler an attractive subject for further research in the fields of materials science, electronics, and energy. In summary, $LiGa_2Ir$ Heusler is a material with immense potential and holds promise for many exciting developments in the near future.

AUTHOR INFORMATION

Corresponding Author

Md. Arif Ul Islam − *Department of Physics, University of Barishal, Barishal 8200, Bangladesh; Department of Electrical and Mechanical Engineering, Nagoya Institute of Technology, Nagoya 466-8555, Japan;* orcid.org/0000-0002-6857-4727; Email: m.islam.622@stn.nitech.ac.jp

Authors

Md. Rasidul Islam − *Department of Electrical and Electronic Engineering, Bangamata Sheikh Fojilatunnesa Mujib Science & Technology University, Jamalpur 2012, Bangladesh*

Ovijit das − *Department of Materials Science and Engineering, Khulna University of Engineering & Technology, Khulna 9203, Bangladesh*

Shinya Kato − *Department of Electrical and Mechanical Engineering, Nagoya Institute of Technology, Nagoya 466-8555, Japan*

Naoki Kishi − *Department of Electrical and Mechanical Engineering, Nagoya Institute of Technology, Nagoya 466-8555, Japan;* orcid.org/0000-0003-2709-3078

Tetsuo Soga − *Department of Electrical and Mechanical Engineering, Nagoya Institute of Technology, Nagoya 466-8555, Japan*

Complete contact information is available at: https://pubs.acs.org/10.1021/acsomega.3c01534

Notes

The authors declare no competing financial interest.

ACKNOWLEDGMENTS

This research was self-funded and received no external financial support.

REFERENCES

(1) Abdul Shukoor, V.; Sarwan, M.; Singh, S. High Pressure Structural, Elastic and Electronic Properties of a New Half Heusler Compound: AuYPb. *Phys. B* **2018**, *547*, 83−87.

(2) Sarwan, M.; Gour, A.; Abdul Shukoor, V.; Singh, S. High Pressure Study of Half Huesler Alloy: YPdSb. *AIP Conf. Proc.* **2019**, *2100*, No. 020158.

(3) Zhu, T.; Fu, C.; Xie, H.; Liu, Y.; Zhao, X. High Efficiency Half-Heusler Thermoelectric Materials for Energy Harvesting. *Adv. Energy Mater.* **2015**, *5*, No. 1500588.

(4) Huang, L.; Zhang, Q.; Yuan, B.; Lai, X.; Yan, X.; Ren, Z. Recent Progress in Half-Heusler Thermoelectric Materials. *Mater. Res. Bull.* **2016**, *76*, 107−112.

(5) Felser, C.; Wollmann, L.; Chadov, S.; Fecher, G. H.; Parkin, S. S. P. Basics and Prospective of Magnetic Heusler Compounds. *APL Mater.* **2015**, *3*, No. 041518.

(6) Kojima, T.; Kameoka, S.; Tsai, A. P. Correction to: Heusler Alloys: A Group of Novel Catalysts. *ACS Omega* **2018**, *3*, 9738.

(7) Kojima, T.; Kameoka, S.; Tsai, A. P. Catalytic Properties of Heusler Alloys for Steam Reforming of Methanol. *ACS Omega* **2019**, *4*, 21666−21674.

(8) Kim, C.; Yoo, W.; Bang, H. W.; Lee, S.; Park, Y. C.; Lee, Y. H.; Choi, J.; Jo, Y.; Lee, K.; Jung, M. H. Highly Reduced Saturation Magnetization in Epitaxially Grown Ferrimagnetic Heusler Thin Films. *ACS Omega* **2019**, *4*, 16578−16584.

(9) Govind, B.; Kumar, A.; Bano, S.; Bhardwaj, A.; Misra, D. K. Structural and Magnetic Properties of Ni1+ XMnSb Bulk Heusler Composite Materials. *ACS Omega* **2020**, *5*, 11895−11900.
(10) Bos, J. W. G.; Downie, R. A. Half-Heusler Thermoelectrics: A Complex Class of Materials. *J. Phys.: Condens. Matter* **2014**, *26*, No. 433201.
(11) Asif, M.; Alrashdi, A. O.; Fadhali, M. M.; Afaq, A.; Bakar, A. First-Principles Investigations of Thermoelectric Behavior of RuCrX (X = Si, Ge, Sn). *ACS Omega* **2022**, *7*, 45353−45360.
(12) Chen, X.; Zhang, X.; Gao, J.; Li, Q.; Shao, Z.; Lin, H.; Pan, M. Computational Search for Better Thermoelectric Performance in Nickel-Based Half-Heusler Compounds. *ACS Omega* **2021**, *6*, 18269−18280.
(13) Lin, S. Y.; Chen, M.; Yang, X. B.; Zhao, Y. J.; Wu, S. C.; Felser, C.; Yan, B. Theoretical Search for Half-Heusler Topological Insulators. *Phys. Rev. B* **2015**, *91*, No. 094107.
(14) Tavares, S.; Yang, K.; Meyers, M. A. Heusler Alloys: Past, Properties, New Alloys, and Prospects. *Prog. Mater. Sci.* **2023**, *132*, No. 101017.
(15) Everhart, W.; Newkirk, J. Mechanical Properties of Heusler Alloys. *Heliyon* **2019**, *5*, No. e01578.
(16) Hao, Z. P.; Liu, R.; Fan, Y. H.; Wang, L. L. First-Principles Calculations of a New Half-Metallic Heusler Alloy FeCrAs. *J. Alloys Compd.* **2020**, *820*, No. 153118.
(17) Wei, X. P.; Chu, Y. D.; Sun, X. W.; Deng, J. B.; Xing, Y. Z. Stability, Electronic, Magnetic and Pressure Effect of Half-Heusler Alloys CNaCa and SiNaCa: A First-Principles Study. *Superlattices Microstruct.* **2014**, *74*, 70−77.
(18) Islam, M. A.; Islam, M. R.; Rahaman, M. Z.; Soga, T. First-Principles Study of Physical, and Superconducting Properties of Newly Discovered Full-Heusler Compound MgPd2Sb. *Phys. Scr.* **2022**, *97*, No. 125705.
(19) Jin, T.; Jung, Y. Recent Progress in Computational Discovery of Heusler Alloys. *Bull. Korean Chem. Soc.* **2022**, *43*, 484−491.
(20) Jin, T.; Jung, Y. Classifying Intermetallic Tetragonal Phase of All-d-Metal Heusler Alloys for Catalysis Applications. *Top. Catal.* **2022**, *65*, 208−214.
(21) Górnicka, K.; Kuderowicz, G.; Winiarski, M. J.; Wiendlocha, B.; Klimczuk, T. Superconductivity in LiGa2Ir Heusler Type Compound with VEC = 16. *Sci. Rep.* **2021**, *11*, No. 16517.
(22) Pani, M.; Pallecchi, I.; Bernini, C.; Ardoino, N.; Marré, D. Synthesis and Structural Characterization of Sb-Doped TiFe2Sn Heusler Compounds. *J. Mater. Eng. Perform.* **2018**, *27*, 6314−6321.
(23) Islam, M. A.; Rahaman, M. Z.; Sen, S. K. A Comparative Study of Hydrostatic Pressure Treated Environmentally Friendly Perovskites CsXBr3 (X = Ge/Sn) for Optoelectronic Applications. *AIP Adv.* **2021**, *11*, No. 075109.
(24) Asrafusjaman, M.; Hasan, M.; Islam, M. A.; Hossain, A. K. M. A. Pressure-Induced Semiconductor-to-Metallic Transition of Monoclinic KCa2Nb3O10 Layered Perovskite: A Theoretical DFT Insight. *Cryst. Res. Technol.* **2023**, *58*, No. 2200262.
(25) Islam, M. R.; Islam, A. S. M. J.; Liu, K.; Wang, Z.; Qu, S.; Zhao, C.; Wang, X.; Wang, Z. Strain-Induced Tunability of the Optoelectronic Properties of Inorganic Lead Iodide Perovskites APbI3 (A = Rb and Cs). *Phys. B* **2022**, *638*, No. 413960.
(26) Islam, M. A.; Islam, J.; Islam, M. N.; Sen, S. K.; Hossain, A. K. M. A. Enhanced Ductility and Optoelectronic Properties of Environment-Friendly CsGeCl3 under Pressure. *AIP Adv.* **2021**, *11*, No. 045014.
(27) Islam, M. R.; Mojumder, M. R. H.; Moshwan, R.; Islam, A. S. M. J.; Islam, M. A.; Rahman, M. S.; Kabir, M. H. Strain-Driven Optical, Electronic, and Mechanical Properties of Inorganic Halide Perovskite CsGeBr3. *ECS J. Solid State Sci. Technol.* **2022**, *11*, No. 033001.
(28) Zhou, Y.; Dong, Z.-Y.; Hsieh, W.-P.; Goncharov, A. F.; Chen, X.-J. Thermal Conductivity of Materials under Pressure. *Nat. Rev. Phys.* **2022**, *4*, 319−335.
(29) Telfah, A.; Sâad Essaoud, S.; Baaziz, H.; Charifi, Z.; Alsaad, A. M.; Mais, M. J.; Hergenröder, R.; Sabirianov, R. Density Functional Theory Investigation of Physical Properties of KCrZ (Z = S, Se, Te) Half-Heusler Alloys. *Phys. Status Solidi B* **2021**, *258*, No. 2100039.
(30) Rahaman, M. Z.; Islam, M. A. A Theoretical Investigation on the Physical Properties of SrPd2Sb2 Superconductor. *J. Supercond. Novel Magn.* **2021**, *34*, 1133−1139.
(31) Ayhan, S.; Kavak Balci, G. Ab-Initio Calculations: Structural, Electronic and Elastic Properties of LiX2Ge (X: Rh, Cu, Ni, Pd) Heusler Compounds. *Mater. Res. Express* **2019**, *6*, No. 0865e9.
(32) Clark, S. J.; Segall, M. D.; Pickard, C. J.; Hasnip, P. J.; Probert, M. I. J.; Refson, K.; Payne, M. C. First Principles Methods Using CASTEP. *Z. Kristallogr. - Cryst. Mater.* **2005**, *220*, 567−570.
(33) Segall, M. D.; Lindan, P. J. D.; Probert, M. J.; Pickard, C. J.; Hasnip, P. J.; Clark, S. J.; Payne, M. C. First-Principles Simulation: Ideas, Illustrations and the CASTEP Code. *J. Phys.: Condens. Matter* **2002**, *14*, 2717−2744.
(34) Perdew, J. P.; Burke, K.; Ernzerhof, M. Generalized Gradient Approximation Made Simple. *Phys. Rev. Lett.* **1996**, *77*, 3865−3868.
(35) Vanderbilt, D. Soft Self-Consistent Pseudopotentials in a Generalized Eigenvalue Formalism. *Phys. Rev. B* **1990**, *41*, 7892−7895.
(36) Yang, Z. X.; Fan, X. H.; Li, Z. P.; Liang, H. A Kohn-Sham Scheme Based Neural Network for Nuclear Systems. *Phys. Lett. B* **2023**, *840*, No. 137870.
(37) Simón, L.; Goodman, J. M. How Reliable Are DFT Transition Structures? Comparison of GGA, Hybrid-Meta-GGA and Meta-GGA Functionals. *Org. Biomol. Chem.* **2011**, *9*, 689−700.
(38) Seifert, G. Tight-Binding Density Functional Theory: An Approximate Kohn− Sham DFT Scheme. *J. Phys. Chem. A* **2007**, *111*, 5609−5613.
(39) Hohenberg, P.; Kohn, W. Density Functional Theory (DFT). *Phys. Rev.* **1964**, *136*, B864.
(40) Momma, K.; Izumi, F. VESTA 3 for Three-Dimensional Visualization of Crystal, Volumetric and Morphology Data. *J. Appl. Crystallogr.* **2011**, *44*, 1272−1276.
(41) Kohn, W.; Becke, A. D.; Parr, R. G. Density Functional Theory of Electronic Structure. *J. Phys. Chem. A* **1996**, *100*, 12974−12980.
(42) Chakraborty, D.; Chattaraj, P. K. Conceptual Density Functional Theory Based Electronic Structure Principles. *Chem. Sci.* **2021**, *12*, 6264−6279.
(43) Magnuson, M.; Mattesini, M. Chemical Bonding and Electronic-Structure in MAX Phases as Viewed by X-Ray Spectroscopy and Density Functional Theory. *Thin Solid Films* **2017**, *621*, 108−130.
(44) Al-Mahayni, H.; Wang, X.; Harvey, J.; Patience, G. S.; Seifitokaldani, A. Experimental Methods in Chemical Engineering: Density Functional Theory. *Can. J. Chem. Eng.* **2021**, *99*, 1885−1911.
(45) Prasert, K.; Sutthibutpong, T. Unveiling the Fundamental Mechanisms of Graphene Oxide Selectivity on the Ascorbic Acid, Dopamine, and Uric Acid by Density Functional Theory Calculations and Charge Population Analysis. *Sensors* **2021**, *21*, 2773.
(46) Nelson, R.; Ertural, C.; George, J.; Deringer, V. L.; Hautier, G.; Dronskowski, R. LOBSTER: Local Orbital Projections, Atomic Charges, and Chemical-bonding Analysis from Projector-augmented-wave-based Density-functional Theory. *J. Comput. Chem.* **2020**, *41*, 1931−1940.
(47) Wang, X.; Yao, J. Improvement of the Self-Consistent-Charge Density-Functional-Tight-Binding Theory by a Modified Mulliken Charge. *Theor. Chem. Acc.* **2017**, *136*, No. 124.
(48) Zhang, C.; Li, L.; Yuan, Z.; Xu, X.; Song, Z.; Zhang, Y. R. Mechanical Properties of Siderite and Hematite from DFT Calculation. *Miner. Eng.* **2020**, *146*, No. 106107.
(49) Khan, M. I.; Arshad, H.; Rizwan, M.; Gillani, S. S. A.; Zafar, M.; Ahmed, S.; Shakil, M. Investigation of Structural, Electronic, Magnetic and Mechanical Properties of a New Series of Equiatomic Quaternary Heusler Alloys CoYCrZ (Z = Si, Ge, Ga, Al): A DFT Study. *J. Alloys Compd.* **2020**, *819*, No. 152964.
(50) Born, M. On the Stability of Crystal Lattices. I. *Math. Proc. Cambridge Philos. Soc.* **1940**, *36*, 160−172.
(51) Roknuzzaman, M.; Alarco, J. A.; Wang, H.; Du, A.; Tesfamichael, T.; Ostrikov, K. K. Ab Initio Atomistic Insights into Lead-Free Formamidinium Based Hybrid Perovskites for Photovoltaics and Optoelectronics. *Comput. Mater. Sci.* **2019**, *169*, No. 109118.

https://doi.org/10.1021/acsomega.3c01534
ACS Omega 2023, 8, 21885−21897

(52) Pugh, S. F. XCII. Relations between the Elastic Moduli and the Plastic Properties of Polycrystalline Pure Metals. *London, Edinburgh Dublin Philos. Mag. J. Sci.* **1954**, *45*, 823−843.
(53) Greaves, G. N.; Greer, A. L.; Lakes, R. S.; Rouxel, T. Poisson's Ratio and Modern Materials. *Nat. Mater.* **2011**, *10*, 823−837.
(54) Ranganathan, S. I.; Ostoja-Starzewski, M. Universal Elastic Anisotropy Index. *Phys. Rev. Lett.* **2008**, *101*, No. 055504.
(55) Ledbetter, H.; Migliori, A. A General Elastic-Anisotropy Measure. *J. Appl. Phys.* **2006**, *100*, No. 063516.
(56) Zener, C. M.; Siegel, S. Elasticity and Anelasticity of Metals. *J. Phys. Chem. A* **1949**, *53*, 1468.
(57) Gaillac, R.; Pullumbi, P.; Coudert, F. X. ELATE: An Open-Source Online Application for Analysis and Visualization of Elastic Tensors. *J. Phys.: Condens. Matter* **2016**, *28*, No. 275201.
(58) Islam, J.; Rahman, M. A.; Hossain, A. K. M. A. Physical and Superconducting Properties of Chiral Noncentrosymmetric TaRh2-B2and NbRh2B2: A Comprehensive DFT Study. *ACS Appl. Electron. Mater.* **2022**, *4*, 1143−1152.
(59) Islam, J.; Farjana, N.; Islam, M. D.; Shabnam, S.; Rahman, M. A. Effect of Pressure on the Superconducting Transition Temperature and Physical Properties of CaPd2P2: A DFT Investigation. *ACS Omega* **2022**, *7*, 21528−21536.
(60) Açıkkalp, E. Entransy Analysis of Irreversible Heat Pump Using Newton and Dulong−Petit Heat Transfer Laws and Relations with Its Performance. *Energy Convers. Manage.* **2014**, *86*, 792−800.
(61) Andritsos, E. I.; Zarkadoula, E.; Phillips, A. E.; Dove, M. T.; Walker, C. J.; Brazhkin, V. V.; Trachenko, K. The Heat Capacity of Matter beyond the Dulong−Petit Value. *J. Phys.: Condens. Matter* **2013**, *25*, No. 235401.
(62) Rahaman, M. Z.; Rahman, M. A. Novel 122-Type Ir-Based Superconductors BaIr2Mi2 (Mi = P and As): A Density Functional Study. *J. Alloys Compd.* **2017**, *711*, 327−334.
(63) Fan, Q.; Liu, C.; Yang, J. Theoretical Prediction of the Mechanical and Thermodynamic Characteristics of Fe2MnGa Heusler Compounds with Different Crystal Phases. *Results Phys.* **2022**, *38*, No. 105567.
(64) Kholil, M. I.; Bhuiyan, M. T. H. Electronic, Elastic, Vibrational and Superconducting Properties of a Ternary Superconductors LaIrP (P = P, As): Insights from DFT. *Solid State Commun.* **2020**, *322*, No. 114053.
(65) Mao, X.-C.; Liu, K.; Hou, B.-S.; Tan, J.; Zhou, X.-L. Theoretical Investigation of the Structural, Elastic, and Thermodynamic Properties of MgAl2O4 Spinel under High Pressure. *J. Phys. Soc. Jpn.* **2016**, *85*, No. 114605.
(66) de Gennes, P. G. Boundary Effects in Superconductors. *Rev. Mod. Phys.* **1964**, *36*, 225.
(67) de Gennes, P. G. An Analogy between Superconductors and Smectics A. *Solid State Commun.* **1972**, *10*, 753−756.
(68) Josephson, B. D. Coupled Superconductors. *Rev. Mod. Phys.* **1964**, *36*, 216.
(69) McMillan, W. L. Transition Temperature of Strong-Coupled Superconductors. *Phys. Rev.* **1968**, *167*, 331.
(70) Blawat, J.; Swatek, P. W.; Das, D.; Kaczorowski, D.; Jin, R.; Xie, W. Pd-P Antibonding Interactions in APd2 P2 (A = Ca and Sr) Superconductors. *Phys. Rev. Mater.* **2020**, *4*, No. 014801.
(71) Ram, S.; Kanchana, V.; Vaitheeswaran, G.; Svane, A.; Dugdale, S. B.; Christensen, N. E. Electronic Topological Transition in LaSn 3 under Pressure. *Phys. Rev. B* **2012**, *85*, No. 174531.
(72) Gillani, S. S. A.; Ahmad, R.; Zeba, I.; Islah-u-din; Shakil, M.; Rizwan, M.; Rafique, M.; Sarfraz, M.; Hassan, S. S. Effect of External Pressure on the Structural Stability, Electronic Structure, Band Gap Engineering and Optical Properties of LiNbO3: An Ab-Initio Calculation. *Mater. Today Commun.* **2020**, *23*, No. 100919.
(73) Ahmed, T.; Roknuzzaman, M.; Sultana, A.; Biswas, A.; Alam, M. S.; Saiduzzaman, M.; Hossain, K. M. Physical Properties of Rare Earth Perovskites CeMO3 (M = Co, Cu) in the Context of Density Functional Theory. *Mater. Today Commun.* **2021**, *29*, No. 102973.
(74) Green, M. A.; Jiang, Y.; Soufiani, A. M.; Ho-Baillie, A. Optical Properties of Photovoltaic Organic−Inorganic Lead Halide Perovskites. *J. Phys. Chem. Lett.* **2015**, *6*, 4774−4785.
(75) Hadi, M. A.; Vovk, R. V.; Chroneos, A. Physical Properties of the Recently Discovered Zr2 (Al1− x Bi x) C MAX Phases. *J. Mater. Sci.: Mater. Electron.* **2016**, *27*, 11925−11933.
(76) Afzal, M. A. F.; Hachmann, J. Benchmarking DFT Approaches for the Calculation of Polarizability Inputs for Refractive Index Predictions in Organic Polymers. *Phys. Chem. Chem. Phys.* **2019**, *21*, 4452−4460.

https://doi.org/10.1021/acsomega.3c01534
ACS Omega 2023, 8, 21885−21897